A model of uniform cortical composition predicts the scaling laws of the mammalian cerebrum

Marc H.E. de Lussanet[a,b,c,*], Kim J. Boström[a], Heiko Wagner[a,b,e]

[a] *Movement Science, Westf. Wilhelms-Universität Münster*
[b] *Otto Creutzfeldt Center for Cognitive and Behavioral Neuroscience, Westf. Wilhelms-Universität Münster*
[c] *ORCID MdL: 0000-0003-3754-6675*
[d] *ORCID KB: 0000-0001-5966-458X*
[e] *ORCID HW: 0000-0002-5470-5044*

Abstract

The size of the mammalian cerebrum spans more than 5 orders of magnitude. The smallest cerebrums have a smooth (lissencephalic) cortical surface, which gets increasingly folded (gyrencephalic) with cerebral size. Further, the proportion of white-to-gray matter volume increases with the total volume. These scaling relations have unusually little variation. It remains an open question, why this is so. Here, we show that almost all variance is explained by assuming a homogeneous composition of the cortex across mammals. On the basis of this assumption we derive quantitative computational models. The first model predicts the cortical surface area from the gray and white matter volume. A single free parameter, for the height of cortical columns $\lambda = 2.9mm$, $r^2 = 0.996$). The second model predicts the white matter volume as a function of the gray volume and the cerebral size (two parameters, $r^2_W = 0.997$, $r^2_G = 0.9997$). The models are validated by predicting the effective cortical thickness and the folding parameter κ. The results accurately predict the human intraspecific variation of the surface relations. We find a reduced λ for cetaceans. Preterm human infants do not follow the model. We also find deviations of gray and white matter volume for large cerebrums. Overall, the models thus show how the regular architecture of the cortex shapes the cerebrum.

Significance statement

The mammalian cerebrum shows a vast distribution in size, from 10 mm^3 to over 5 liters. Across this range highly regular scaling relations have been found, e.g., for volume of grey and white matter and cortical surface. Despite considerable efforts, these scaling relations are still not understood. Here, we develop a model, assuming that cortex and the white matter have a uniform composition across mammals of every size, and independent of phylogeny. On the basis of this simple assumption we could accurately predict the scaling relations. The results show that humans are in the normal scaling range from birth age. Cetaceans are the only clade to show a reduced cortical thickness parameter.

Preprint Server: BioRxiv

Classification: **Biological Sciences**: Neuroscience, Systems Biology

Keywords: mammal; cortex; cerebrum; scaling laws; computational model

*Corresponding author:
lussanet@wwu.de
Phone: +49 151 180 69 156

1. Introduction

Scaling relations are a classic field of evolutionary biology. The mammalian cerebrum ranges in size from about 10 mm^3 (pygmy shrew) to more than 5 dm^3 (fin whale, Pilleri and Gihr, 1970), i.e., more than 5 orders of magnitude. The scaling relations of the mammalian cerebrum are extraordinary because various parameters such as volume, surface, and proportion of gray matter (Changizi, 2001; Hofman, 1985; Cuntz et al., 2012) all show trends with very little deviation across several orders of magnitude and independently of phylogenetic relationships (e.g. Hofman, 1989; Zhang and Sejnowski, 2000). This is in contrast to other scaling relations such as the encephalisation (expressed as brain-, cerebral- or cortical mass to body volume) which can vary by twentyfold between species of the the same body mass (Boddy et al., 2012), and which have different scaling relations within species versus between species, and between phylogenetic groups (Boddy et al., 2012; Manger et al., 2012).

The tight scaling relations suggest a simple scaling mechanism that depends on only a few parameters. It is tempting to assume isometric scaling in some form, but this is not the case (Braitenberg, 2001). Understanding the common mechanisms that underlie the scaling relations will help to formulate scaling laws; to identify exceptions from these laws and thus help to understand evolutionary differences between species and brain regions (Rakic, 2009; Van Essen et al., 2019).

One remarkable scaling relation of the mammalian cerebrum exists between volume and total surface area (Hofman, 1985). Under the assumption that the overall shape of the cerebrum is scale-independent (de Lussanet, 2015), this relation is equivalent to the relation between exposed surface area and total surface area, which is sometimes expressed as a ratio (called folding index or cephalization index: Manger, 2006). A second remarkable scaling relation has been found between the volume of gray and white matter (Zhang and Sejnowski, 2000). More recently, a fractal-like relation between the total surface, the exposed surface, and the ratio of the volume to the exposed surface has been proposed (Mota and Herculano-Houzel, 2015). It was shown however, that this scaling relation amounts to the simpler assumption that the folding index times the proportion of gray matter volume would be approximately constant (de Lussanet, 2016).

According to the cortical surface to volume scaling relation, the total surface area of the cortex increases over-proportionately with the volume of the cerebrum. Consequently, the cortex of small cerebrums (such as that of mice) have a smooth surface, which is called *lissencephalic*, whereas the cortex of large cerebrums (such as that of humans) is increasingly folded, which is called *gyrencephalic*.

The tension hypothesis (Van Essen, 1997) proposes a mechanism for the development of the cortical folding pattern. The axons that connect neighboring regions (and which are oriented parallel to the cortical surface) pull the cortex into a convex curvature to form gyri. On the basis of numerical simulations and dynamic tensor imaging (DTI) it has been questioned if, indeed, the axonal tension hypothesis can explain the convex curvatures of the gyri (Xu et al., 2010).

An alternative tension hypothesis has proposed that the axons that are oriented perpendicular to the cortical surface evoke a buckling pattern of the cortical surface, especially in large cerebrums. This hypothesis is supported by a numerical computational model (Manyuhina et al., 2014). Manyuhina et al. argued, that the radial and tangential tension hypotheses might be complementary, and we agree with that view. The cortical innervation is not homogenous, but the bundles primary innervation fields are localized for each sense, as are the primary motor outputs. Thus, an extended tension hypothesis (ETH) combines all three effects: the two tension hypotheses and the bundled primary fields should suffice to explain the development of gyrification. The maturing zones either receive sensory input or generate motor output, and respectively form the primary sensory and motor areas present in all mammals. As the cerebrum grows, so we hypothesize, the tension in the long-range axonal connections keeps the maturing zones from growing outwards and so they fold inwards and form sulci, while the growth zones between the maturing zones grow outwards and form gyri (Fig. 1A-C). The width of the gyri is constrained by the height of the cortical columns and the relatively dense short-range connections. As the apex of a gyrus grows outward, it becomes wider, the flanks become separated, and another sulcus is formed (Fig. 1C).

It is widely accepted that the mammalian cerebral cortex shows a highly homogeneous composition of layers and neuronal cortical columns. The layers differ between regions of the mature cortex, but always show the developmental state of

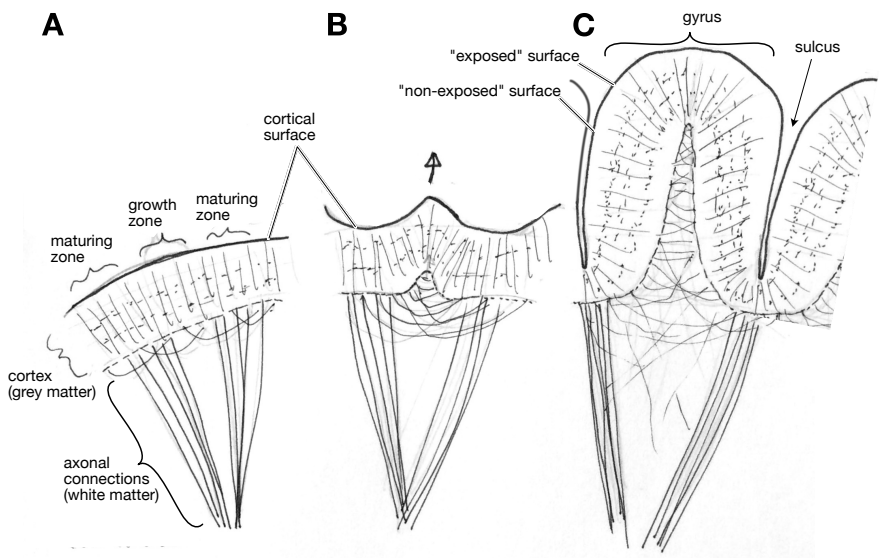

Figure 1: Sketch of the proposed extended tension hypothesis (ETH) with regional growth zones. A. In the developing cortex, growth zones alternate with maturing zones. The latter possess more dense long-range axonal connections. B. When the cerebrum increases in size, tension in the long-range axonal connections will restrain outward movement of matured zones. C. Consequently, the matured zones form sulci. The width of the gyri is restrained by the tension in the short-range connections between the cortex on the neighboring flanks.

six layers at some time (Brodmann, 1913). Cortical columns integrate the layers perpendicularly to the cortical surface, and are regarded as computational units, which are highly uniform across the size range of the cerebrum (Rakic, 1995). It is thought that the volume of cortical columns is independent of the local curvature of the cortical surface (Bok, 1929). Evidence from precise counting studies across species suggest that the number of cortical neurons per square millimeter is invariably close to $\sim 10^5$ per mm^2 (Rockel et al., 1980; Carlo and Stevens, 2013).

White matter contains the myelinated long-distance axonal connections. To answer the question how the volume of the white matter relates to the gray matter it is, therefore, essential to know how the diameter of axonal connections depends on the length of the axons. For example, it is well known that the myelin sheath increases the signal transmission velocity linearly with the axonal radius (Perge et al., 2009). Many invertebrates possess a few giant axons for long-range startle responses. Accordingly, one might expect large mammalian cerebrums to have axons with a wide diameter.

However, since the axonal volume increases quadratically with its diameter, a bundle of many narrow axons will transmit more information per second than a bundle with the same cross-section, which consists of a few wide axons. Moreover, due to noise, the efficiency of information transfer decreases with the spike rate according to Shannon's information theory (Balasubramanian et al., 2001). Indeed, it has been estimated from the frog's retina that each cell type transmits approximately the same amount of information independent of its axonal diameter, so that thin fibres transmit vastly more information per summed cross-sectional area than thick ones (Koch et al., 2006). Consistently, the axonal width distribution in the mammalian brain seems to be largely independent of brain size (Perge et al., 2012).

In the present study we aim to explain the empirical scaling relations of the mammalian cerebrum. We hypothesise that valid scaling laws can be formulated on the basis of a simple growth rule and the uniform structure of the cortical building blocks and the scale-independent distribution of axonal widths. Below we derive a model that predicts the total cortical surface area on the basis of the grey and white matter volume. One parameter is fitted, i.e., the average height of the cortical columns. We hypothesize that a single scaling relation holds for the entire size range of mammalian cerebrums, independent of phylogenetic relations. The model is fitted to existing empirical data of the cerebral

volume to surface area.

Similarly, to calculate the white matter volume, we hypothesize that the distribution of axon diameters in the white matter is independent of cerebral size and that the number of axons scales linearly with the grey matter volume. This second model with two free parameters will be fitted to existing data of cerebral grey and white matter volumes.

The models will be validated using existing empirical data of 1st the exposed surface area to total surface area, 2nd we hypothesize that the same scaling relation holds within a species, i.e., the human cerebrum, 3rd the ratio of grey matter volume and surface area to cerebral volume (*effective thickness*) and 4th the folding parameter (κ).

Third, having developed a theory-based and validated tool allows to investigate exceptions. The tension hypotheses are developmental ones, and so are predicted to hold even for the growing cerebrum after birth. However, before birth, there is no need for functional cerebral sensorimotor control and so it is expected that preterm infants deviate from the predicted relationships. Also, we will discuss the results for cetaceans in the light of earlier results.

2. Modelling

2.1. Surface to volume scaling relation

This model will result in two equations, one for convoluted or *gyrencephalic* cerebrums (Eq. [7]) and one for smooth or *lissencephalic* cerebrums (Eq. [8]). The predicted relation is the maximum of these relations.

The outer ("exposed") surface of the cerebrum differs from the deeper parts: 1. it does not contain any white matter, only gray cortex; 2. it is formed of the apex of gyri, so that the cortex in this border region is more strongly curved than the cortex inside the sulci.

We can thus distinguish the cortex (with volume G) into a convex gyral border of volume G_B and thickness λ, and a more planar to concave sulcal core of volume G_C and a radius $R-\lambda$. Since the fundus of the sulcus occupies a very small part of the total cortical surface, it can be neglected and it follows that the area of the core surface obtains

$$A_C = G_C/\lambda. \tag{1}$$

The volume V_C of the core consists of gray and white matter, so we have $V_C = G_C + W$, with W from Equation [12]. Simultaneously, the core volume is approximately equal to the volume of a ball of radius $R-\lambda$ (see above), so

$$\begin{aligned} V_C &= \tfrac{4}{3}\pi\left(R-\lambda\right)^3 \\ &= 4\pi\left(\tfrac{1}{3}R^3 - R^2\lambda + R\lambda^2 - \tfrac{1}{3}\lambda^3\right). \end{aligned} \tag{2}$$

Using Eq. [1] and [2], the core surface area A_C can thus be expressed as

$$\begin{aligned} A_C &= \frac{V_C - W}{\lambda} \\ &= 4\pi\left(\tfrac{1}{3}R^3/\lambda - R^2 + R\lambda - \tfrac{1}{3}\lambda^2\right) - \frac{W}{\lambda}. \end{aligned} \tag{3}$$

The cerebral border region V_B is free of white matter but composed entirely of the convex part of the gyri. Due to the convexity, the cortical columns are not column-shaped as in the sulcal regions of the cortex, but rather pie-shaped. Assuming that the cortical columns in the convex regions have the same volume as those in the flat, sulcal regions, the cortical surface per cortical column should be about twice as large in the cerebral border region. For the cortical surface in the border region A_B that:

$$A_B = \frac{2V_B}{\lambda}. \tag{4}$$

The border volume is the cerebral volume minus the core volume, hence $V_B = V - V_C$. Let us approximate the cortical volume V by the volume of a ball of radius R, hence neglecting the sphericity, so $V = \frac{4}{3}\pi R^3$, and let us use Eq. [2] for the core volume V_C, we then arrive at

$$\begin{aligned} V_B &= V - V_C \\ &= \tfrac{4}{3}\pi R^3 - \tfrac{4}{3}\pi(R-\lambda)^3. \end{aligned} \tag{5}$$

Inserting the above expression for V_B into Eq. [4], we obtain

$$A_B = 4\pi\left(2R^2 - 2R\lambda + \tfrac{2}{3}\lambda^2\right). \tag{6}$$

Using the above equation and Eq. [3], the total cortical surface of a gyrencephalic cerebrum reads

$$\begin{aligned} A_{\text{gyr}} &= A_B + A_C \\ &= 4\pi\left(\tfrac{1}{3}R^3/\lambda + R^2 - R\lambda + \tfrac{1}{3}\lambda^2\right) - \frac{W}{\lambda}, \end{aligned} \tag{7}$$

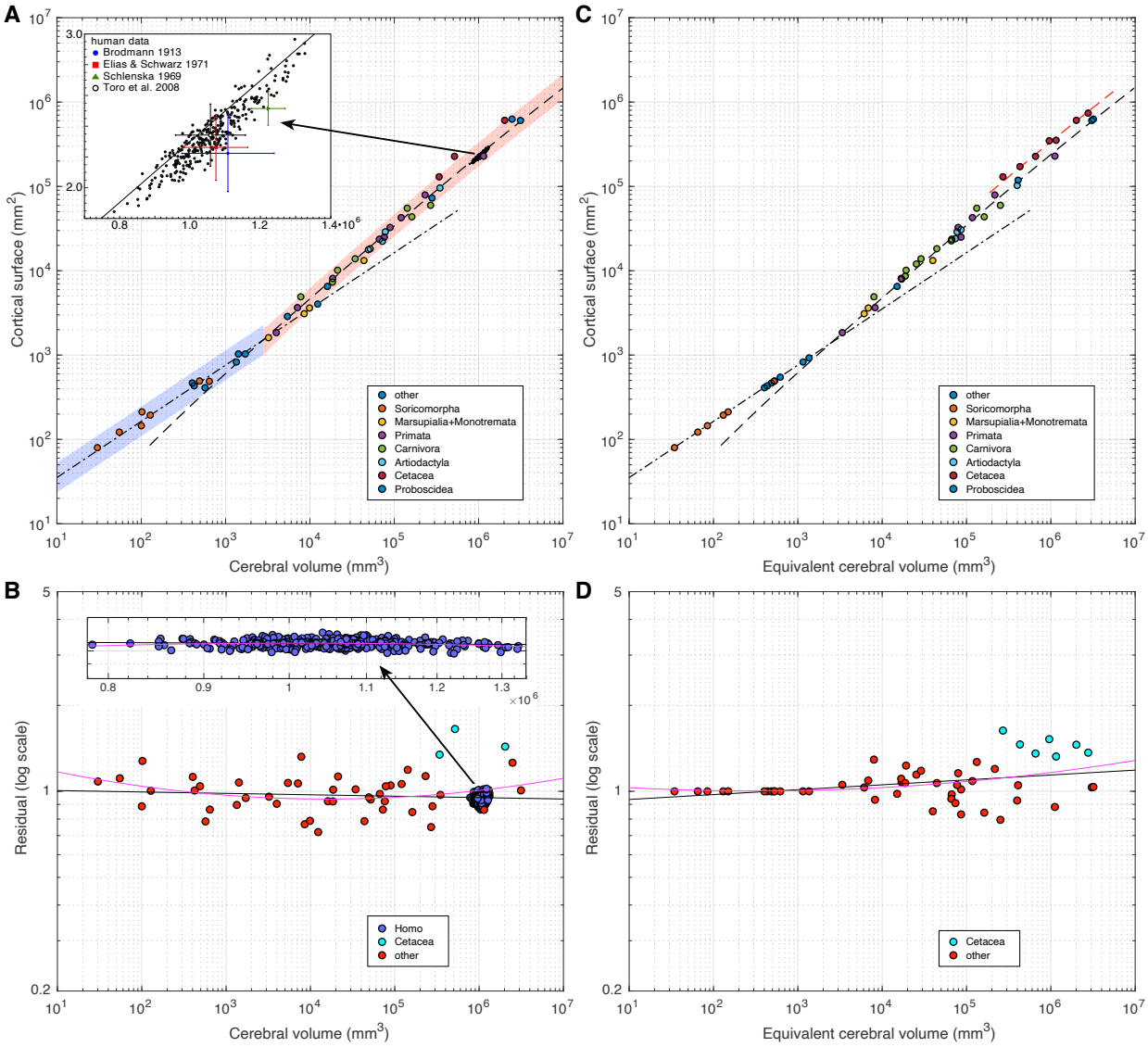

Figure 2: Results of model 3 for the cortical surface in relation to the cerebral volume. A. Gyrencephalic cerebrums scale with Eq. [7] (dashed curve); lissencephalic cerebrums scale with Eq. [8] (dash-dotted curve). Shaded regions show a factor 1.5 for the sphericity, s (blue) and cortical thickness λ (red) parameters. Note that the set of human MRI data (cloud of dots), was not included for the data fitting. Inset: The human data by literature source. B. The residual on log scale as a function of the cerebral volume. Black lane and lilac curve: linear and quadratic regression, respectively (including the cetaceans, blue dots). The inset shows the human MRI data with the same vertical scale. C. The same model; the equivalent volume was calculated from the exposed surface area, using the exposed surface to volume ratio (A_{exp}, see Fig. S1 and Methods section). The black curves are the same as in Panel A. The red dashed curve shows the model fitted to just the cetaceans. D. The residual for panel D. Note, that the exposed surface equals cortical surface for lissencephalic cerebrums. The cetaceans are shown with blue dots.

where $R = \sqrt[3]{\frac{3}{4}\pi V}$ (because $V = \frac{4}{3}\pi R^3$ as explained above).

If the radius of the cerebrum is smaller than the thickness of the border, the cerebrum is smooth (lissencephalic). In that case, the cortical surface equals the spherical volume and surface relations ($V = \frac{4}{3}\pi R^3$ and $A = 4\pi R^2$), so

$$A_{\text{liss}} = (36\pi)^{1/3} s V^{2/3}, \tag{8}$$

with the dimensionless sphericity constant $s = 1.56$ to correct for the deviation from a perfect sphere of the cortical hemispheres (Fig. S1).

Equations [7] and [8] thus predict the scaling relation for the cortical surface. The intersection point between the two equations is the transition between them, such that

$$A = \max\{A_{\text{liss}}, A_{\text{gyr}}\}. \tag{9}$$

The white matter volume W (eqn. [7]) can, unfortunately, not be obtained directly from published data. Instead, the white matter volume will be estimated using eqn. [12] below. The model has thus just one single free parameter λ to be fitted against the data.

2.2. Gray and white matter volumes

Thus, assuming that the distribution of axonal diameters in the white matter is independent of brain size, the volume of the axonal connections increases linearly with the distance between the regions that they connect. The summed cross-section A_W of the axonal connections scales with the number of neurons in the gray matter, which in turn scales with the gray matter volume. It follows that the summed cross-section A_W scales with the gray matter volume. Since the white matter volume W is proportional to the mean axonal length $\bar{l}$ times the summed cross section A_W, we obtain

$$W = \bar{l} A_W \propto \bar{l} G. \tag{10}$$

Part of the axonal connections will be intra-gyral, so that their length is independent of the size of the cerebrum. On the other hand, the length of long-distance extra-gyral connections will scale with the radius R of the cerebrum. Given our central assumption that the compositional scheme of the cortex, as outlined above, is independent of the size of the brain, the proportion of short-distance and long-distance connections should be constant with respect to the cerebral radius R. Given the characteristic overall shape of the cerebrum, the total volume of the cerebrum will scale with the cube of R, so the cerebral volume obtains $V = cR^3$, with c being a shape constant. The white matter volume

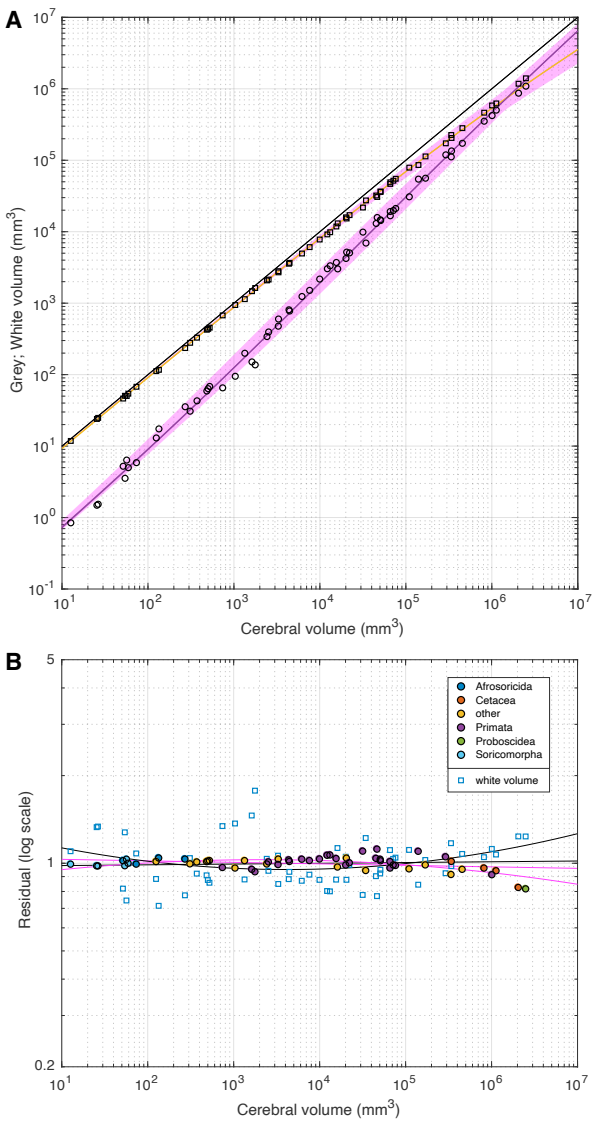

Figure 3: Model for gray and white matter volumes, fitted to the dataset of Zhang and Sejnowski (2000). According to Model 2 (Eq. [12]), the white matter volume scales to the cerebral size in two ways: long-range extra-gyral connections scale with the cerebral radius, and short-range, intra-gyral connections scale with the total cerebral surface. A. The fitted relation on a log-log scale. B. The residual on a log scale as a function of the cerebral volume. Note, that the residual has log-units. Black curves: linear and quadratic regressions to the white matter residual; purple curves: the same for the gray matter.

W is the sum of the local and global connections, and so we obtain

$$W = G\left(a\sqrt[3]{\frac{V}{c}} + b\right). \tag{11}$$

Since $V = W + G$ we obtain for the gray and white matter volume, with $\hat{a} = a/\sqrt[3]{c}$:

$$G = \frac{V}{\hat{a}\sqrt[3]{V} + b + 1},$$
$$W = \frac{V(\hat{a}\sqrt[3]{V} + b)}{\hat{a}\sqrt[3]{V} + b + 1}. \tag{12}$$

3. Results

The model for the relation of cortical surface to cerebral volume has just one single free parameter λ, which describes the cortical thickness. Fitting this parameter to the averages per species (excluding the human MRI data) and using a mean sphericity of $s = 1.57$ (Fig. S1), resulted in $\lambda = 2.81$ mm (N=47, $r^2 = 0.996$; Fig. 2A). (The cetacean $\lambda = 1.9$. Without the cetaceans, the fit would be even slightly better: $\lambda = 2.94$ mm, $r^2 = 0.997$.) The residuals (log units) are shown in Panel B (curvature: $P < .001$). The fitting of the individual measurements in the human dataset resulted in $\lambda = 2.97$ mm ($r^2 = 0.962$; Panel A-inset). The corresponding residual is shown in the inset, curvature: $P < .01$. For a part of the measurements (N=51 species) the exposed cerebral surface area was reported. Using σ, the cerebral volume was estimated for these measurements (Fig. 2C). The residuals (Panel D) systematically increase with cerebral volume ($P < .01$). Note, that the lissencephalic cerebrums are exactly on the predicted relation because cortical and exposed surface area are equal.

Model 2. The gray and white matter volume model, Eq. [12], describes the data very well, with the best-fitting parameter values $\hat{a} = 0.00811$, $b = 2.060$ (with $r_W^2 = 0.997$; $r_G^2 = 0.9997$). The resulting two relations are plotted in Figure 3A. The residuals (log units) were generally much smaller for gray then for white matter volume (Fig. 3B: gray slope: $P < .05$, curvature: $P < .01$; white curvature: $P < .05$).

Two existing relations can be predicted on the basis of the current models. The *effective cortical thickness* is defined as the ratio of estimated gray matter volume (eqn. [12]) to cortical surface area (eqn. [7]) represents (cf. de Lussanet, 2016), and is shown in Fig. 4A. The model (red dashed curve) describes the general trend in the empirical data, but the data have considerable variation for gyrencephalic cerebrums.

The folding parameter κ was predicted to be a constant by the model of (Mota and Herculano-Houzel, 2015), but this prediction was falsified on a statistical basis (de Lussanet, 2016). The folding parameter can also be predicted on the basis of the equations [12] and [7] and the spphericity (see Supplement). The prediction, along with the empirical data (cg. Mota and Herculano-Houzel, 2015), are shown in Figure 4B.

4. Discussion

We have proposed a unified theoretical concept to explain the scaling relations of white matter volume and cerebral surface area. The basis of the

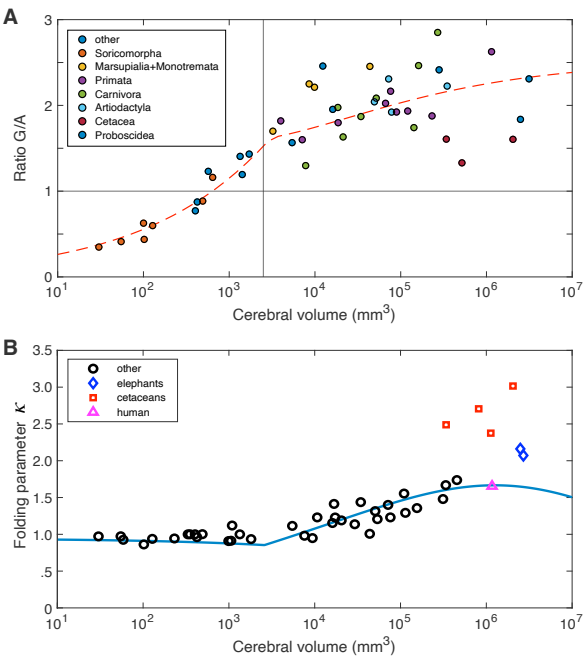

Figure 4: Predictions for the effective cortical thickness (A) and folding parameter κ (B). A. The effective cortical thickness, i.e., the ratio of gray volume to cortical surface area G/A as a function of the cerebral volume ($\log(V)$). Vertical line: transition to convoluted cerebrums. Dashed curve: Model prediction (see text). B, The folding parameter κ is the proportion of grey volume times the folding index (de Lussanet, 2016), as calculated from the models along with the data from (Mota and Herculano-Houzel, 2015). Blue squares: cetaceans, red rhombus: African elephants.

concept is simple: the regular scaling patterns of the mammalian cerebrum are caused by, and reflect, the highly regular and uniform composition of the cortex into a fixed number of (six) layers and into a variable number of cortical columns. The presented models are derived on the basis of these premises.

The mechanical mechanism that leads to cortical folding is an old question whose answer has been sought in differential growth (Le Gros Clark, 1945; da Costa Campos et al., 2020, see Striedter et al., 2015 for a review). Tension hypotheses (ETH) propose that the anisotropy of the orderly arrangement of white matter and the growth tension in axons might be a driving force to produce convex curvatures of the gyri (Van Essen, 1997; Manyuhina et al., 2014). Moreover, the clustering of long-range axonal connections by each of the senses and by the motor outputs will prime such folding, so that we predict a hierarchical pattern of cortical folding (Garcia et al., 2018). Thus, first order sulci are also the most consistent ones across the size range, and these should coincide with the primary sensory and motor areas. Indeed, the median fissure (olfaction), the calcarine sulcus (vision), the lateral sulcus (vestibular and audition), and the central sulcus (somatosensation and motor) are the deepest and most constant sulci across the mammalian cerebrum. The underlying assumption of the model is that the functional map of the mammalian cortex shows a uniform plan across the entire class, which is widely accepted (Kaas, 2011).

This hierarchical folding rule predicts that fractal-like pattern. This notion has existed since several decades (Hofman, 1991; Mota and Herculano-Houzel, 2015; Stoop et al., 2013), but could not be proven yet (de Lussanet, 2016). A very simple model that implements such a simple fractal-like growth rule, in addition to the ETH, describes the scaling of the volume-surface relation already remarkably well (Fig. S3).

The first model (Eq. [9]), contains just one single free parameter: the cortical thickness λ, while fitting the data really well ($r^2 = 0.996$). Across species the cortical thickness ($\lambda = 2.81$ mm) was very close to the intraspecific value for humans ($\lambda = 2.97$ mm). This latter value is within the range reported by Bok for a single specimen (Bok, 1929). Our value for λ is somewhat higher than the *effective* cortical thickness (i.e., the ratio of $G/A = 2.63$ for humans, cf. Fig. 4A; see also Frangou et al., 2020). This is to be expected because the latter definition neglects that the cortical surface has a convex to convoluted shape.

The second model derives the white matter volume by the additional assumption that the cross-section of white matter per gray matter volume is constant, and that a constant proportion of the white matter connections are connecting locally versus globally. With just two free parameters, the model fits the data well (r^2 equals 0.997 and 0.9997, respectively, see results). The small quadratic trend in the residual suggests that the model slightly overestimates the white matter volume in the smallest and the largest cerebrums. For small cerebrums this is indeed to be expected, when the radius of the cerebrum becomes smaller than the length of the local connections in a gyrencephalic cerebrum. For elephants and pilot whales (the two data points with the largest cerebrum $V \approx 2$ l) the model predicts the white matter volume to be larger than the gray matter volume, which is not the case. Rather, the proportion of white matter seems to saturate around 45% for brains the size of humans and larger.

Zhang and Sejnowski (2000) proposed a model for the grey-to-white matter volume relation on the assumption that the cortical geometry minimizes the overall length of the axonal connections (maximizing compactness), predicting that $W \propto G^{4/3}$. The power of scaling is represented by the slope in a log-log graph. Linear regression on the log-log data resulted in a significantly lower slope of 1.23. By contrast, our model predicts the scaling power well, increasing slightly with cerebral size (from 1.09-1.36).

The folding parameter was proposed by (Mota and Herculano-Houzel, 2015) as a fitting constant of their model assuming optimal free energy in tension for the cortical surface area. De Lussanet 2016 showed that this parameter is better expressed in terms of the proportion of gray matter volume and the folding index: $\kappa = G/V\dot{A}/A_{exp}$. The latter study showed that κ deviates significantly with cerebral size. Here we show, that the folding parameter κ is well predicted by the current models (Fig. 4B), with the exception of cetaceans and elephants, due to the saturation in the grey-white matter volume relation (see above). Thus, the folding parameter provides additional evidence, validating the current modelling approach.

A chronic difficulty of earlier models has been to predict the power of the scaling relations for the cortical surface (Hofman, 1985, 1989; Mota and

Herculano-Houzel, 2015; Xu et al., 2010; Braitenberg, 2001) as well as for the white matter volume (Zhang and Sejnowski, 2000). Hofman (Hofman, 1989) found a slope of 0.83 for a linear regression on convoluted cerebrums. The current model predicts a power of scaling is very close to 0.83 within the size range of $10^4 - 10^7$ mm^3 and a slightly higher power for smaller sizes.

The reasoning underlying the present scaling theory is that across the huge size range, deviations from the general trend are small. It follows that few factors determine the general scaling pattern, so we derived analytic scaling relations. Obviously, this approach involves *simplifications*. For example, the number of neurons (Rockel et al., 1980; Carlo and Stevens, 2013) and the effective cortical thickness (Frangou et al., 2020) are slightly different between the different lobes. However, since such local differences are present across species of different sizes (Rockel et al., 1980), they will average out. Also, the cortical thickness λ depends on the curvedness (Bok, 1929). The model will therefore slightly overestimate the cortical surface area in the border region. On the other hand, it will slightly underestimate the cortical surface in the core region because the core region also contains gyri. The central conclusion is, that, indeed, simple principles can be defined to predict almost the entire variation in white matter volume, cerebral surface area and folding pattern.

One might speculate about deviations (and the absence thereof) with respect to the models. Remarkable is the absence of systematic effects of different literature sources despite the data being collected across an entire century using various methods (cf. supplementary Fig. S2B). One important source of error might be in the conservation artifacts (all studies corrected for those artifacts). The small systematic differences in cortical surface area in human data from conserved specimen (Brodmann, 1913; Elias and Schwartz, 1971) with respect to the in-vivo MRI data (Toro et al., 2008) might be due to the older age of the subjects in the earlier studies, which were analysed post mortem (Fig. 2A, inset). The overall slightly larger volume of Schlenska (1969, N=5) might be due to the small sample and the conservation artifacts. Given that the standard deviations in all four studies are very similar, suggests that the precision of the techniques used is good and relatively small in comparison to the natural variation in cerebral size.

Another remarkable pattern is the lack of phylogenetic trends. In cerebrums larger than human's, the relative contribution of gray and white matter seems to saturate (Fig. 3B). This observation involves the African elephants and cetaceans, and is clearly reflected in the folding parameter κ which the current model even predicts even to go down for very large cerebral sizes. This deviation probably reflects that the assumption that the long-distance connections scale with cerebral radius (eq. [11]), does not hold for very large cerebrums. More data are needed to test this.

The only clade that shows systematic deviations from the cortical surface model (Fig. 2) are cetaceans (Manger et al., 2012; Roth, 2015; Marino et al., 2007). The data strongly suggest that cetaceans have a lower cortical thickness parameter λ (cf. fig. 2C). This is consistent with 40% increased cortical surface area with respect to the entire cerebral volume. For example the number of glia cells, e.g. astrocytes, throughout the cerebrum could be enhanced. Indeed, evidence shows that the large cerebrum cetaceans (and other aquatic mammals) does not provide them with superb cognition or intelligence, a lack of neuronal specialization and prefrontal cortex (Manger, 2006, 2013; Patzke et al., 2015). Rather, the increased brain size seems to reflect a physiological specialisation. Manger (2006) argued that this physiological specialisation is heat production: the mammalian is highly sensitive to minor changes in temperature, so keeping brain warm in cold water should indeed present a major evolutionary pressure.

Humans, on the other hand, are remarkably close to the model fit for both models. This finding is in line with earlier conclusions (Azevedo et al., 2009; Herculano-Houzel, 2012). The data of Toro et al. (Toro et al., 2008) show, moreover, that the model predicts the scaling relation even within the human species well for young adult humans (Fig. 2A-B).

We hypothesized that preterm infants will be below the predicted scaling relation because the cortical thickness decreases with growth. The MRI data of prematurely born infants (Kapellou et al., 2006) suggests that the predicted scaling relation is reached around the age of normal gestation time (38-42 weeks: Fig. 5). According to these data, the cerebrum is lissencephalic until about 10^5 mm, i.e., 50 times the transition to gyrencephaly in adult mammals (Fig. 5). These data thus suggest, that the scaling relation might be accurately predicted across the developmental span for humans post gestation. This is consistent with Wang et al. (2017)

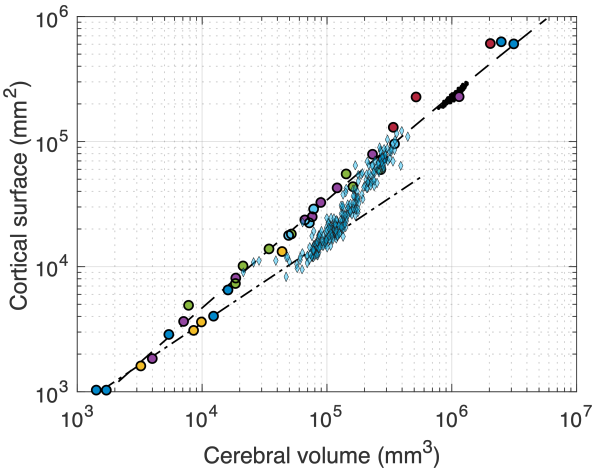

Figure 5: Very premature infants scale differently. The figure shows an inset of Figure 2, with additionally included MRI data of 130 extremely prematurely born infants (blue triangles; gestation week 22-29; normal full term would be 38-42 weeks; Kapellou et al., 2006). Most infants were scanned more than once (n=274). Age range at scan: 23-48 weeks post gestation. The volume-surface relation was much more variable than for the adult population. The smallest cerebrums were lissencephalic until about 10^5 mm, i.e., 50 times the transition to gyrencephaly in adult mammals. From there, a steep increase in cortical surface occurs (the black line represents $A = V^2$). The model curve is reached at a volume of about $2 - 4 \cdot 10^5$ mm, which is only about 1/3 of the average adult volume.

who found that the increase in cortical surface area comes later than the increase in cortical volume.

A considerable number of models have been proposed to explain the cortical folding and the scaling relations of the mammalian cerebrum. Most have not been validated to empirical data (e.g. Le Gros Clark, 1945; Karbowski, 2003; Schlenska, 1974; Jerison, 1979; Hofman, 1985, 1989; Prothero and Sundsten, 1984; Todd, 1982; da Costa Campos et al., 2020; Van Essen, 1997; Mota and Herculano-Houzel, 2012). Other models were validated (e.g. Mota and Herculano-Houzel, 2015; Xu et al., 2010; Braitenberg, 2001; Zhang and Sejnowski, 2000), but failed to explain the empirical data. This state of research is confusing, given that the empirical data show such an unusually clear pattern, which suggests that the scaling relations are governed by just few parameters.

We have here proposed two models that explain the pattern of cerebral folding (gyrification) and white matter volume, on the basis of a single concept, i.e., the homogeneous construction principles. According to this principle, both white matter volume and cortical surface area are simple geometric scaling functions of the gray matter volume. The validation to the available empirical data shows that model and data are fully consistent.

Conclusions

1. Very few simple principles can be defined to predict almost the entire variation in white matter volume, cerebral surface area and folding pattern.
2. Our model is validated by the available empirical data.
3. Our new theory provides strong evidence that uniform cortical composition in mammals drives the most important scaling relations known from the literature.
4. We provide evidence that the cortical surface area and the volume of white matter in the mammalian cortex are governed by the volume of gray matter, probably due the cortex being universally composed of cortical columns and being layered.
5. We propose an extended tension hypothesis (ETH) that explains the general pattern of sulci and why this pattern follows the cortical functional map.
6. The ETH also predicts a fractal-like growth rule and hierarchical patterning of the sulci.
7. The proposed scaling relation is largely independent of phylogenetic relations and even holds within the human species.
8. According to the present view, the regular scaling relations of the cerebrum do not reflect an evolutionary optimum. Rather, the present scaling laws can be formulated on the basis a simple growth rule and the uniform structure of the cortical building blocks.

5. Methods

5.1. Datasets

For the gray and white matter volume data, we used the database of Zhang and Sejnowski (2000), which includes measurements for 59 species of mammals. The cerebral volume and cortical surface area for human cerebrums was measured for 314 young adults on the basis of in-vivo MRI measurements (Toro et al., 2008).

For the database of surface to volume, only measurements from the same specimen were included

(see Supplementary Table). If for a species several measurements were available, these were averaged. Since not all studies measured all parameters, the number of included measurements may differ depending on the included measures. For example: three studies report data for horses, in total 7 specimen. When including cerebral volume and total surface area the mean volume for the horse is 297 cm^3 (N=7), but when including cerebral volume and exposed surface area, the mean volume is 450 cm^3 (N=2), because the exposed surface area was not measured (Mayhew et al., 1996).

The first systematic and accurate measurements of a wide range of mammals have been developed and published by Brodmann and Henneberg (Brodmann, 1913; Henneberg-Neubabelsberg, 1910). The total cortical surface was measured by precisely covering it with pieces of silk paper. Since this method is not easy to apply and is very labour intensive, later measurements tended to use a statistical approach using slides, e.g. counting the number of surface crossings on a grid and applying a correction formula. A further problem is the effect of shrinkage due to conservation in ethanol (e.g. Mayhew et al., 1996). Consequently, it is likely that an important source of variability in the data lies is in the measurement techniques used.

The selection criteria for the inclusion of studies were as follows: 1. Systematic usage of a validated method; 2. Reporting of a range of mammals (not just humans); 3. Reporting of at least the cerebral surface area and the cerebral volume and/or the cerebral outer surface area from the same specimen. Seven studies matched these criteria: (Brodmann, 1913; Schlenska, 1969; Haug, 1970; Elias and Schwartz, 1971; Schlenska, 1974; Mayhew et al., 1996). Finally, the measurements of reported total/outer surface ratio of 1.0 (i.e., lissencephalic cerebrums) were added from Hofman (1985).

Exclusion criteria were applied as follows (see Supplementary Table): 1. Malformed or diseased brains (this applies to some measurements in Brodmann, 1913); 2. excessively deformed brains (Brodmann suspected excessive shrinkage of two brains of Ganese origin); 3. Estimates (e.g., of cerebral volume) that were based on other specimens or taken from the literature; 4. Measures of cerebral volume that do not fit into a sphere of the reported total cortical surface (this applied to Elias and Schwartz, 1971); 5. for *Homo sapiens*, ten statistical outliers from three publications were excluded.

The remaining dataset used in the present study thus includes 141 samples (incl. 29 humans) from 55 species and 17 orders of mammals. The cerebral volume was available in 97 samples and the outer surface of 104 samples. For the fitting a single average per species was calculated: 44 species for the A_c-V_c fit and 51 species for the A_c-A_{exp} fit. In either case, the A_c of a species was calculated over the samples that were available for the second parameter, so that the mean A_c for a given species could differ depending on the fit. The complete data set as well as a commented listing of the excluded measurements is provided for downloading (see Supplementary Table).

5.2. Analysis

The fitting procedures were performed on the mean values of the species, so that each species is represented by just a single value regardless of the number of samples that had been used for the mean. These data were fitted using a least squares fit to the logarithmic data. To estimate the goodness of fit, not only the r^2 were taken, but also the first and second order trends in the residue. Such linear or u-shaped systematic deviations from the model can be important cues for validating the underlying model.

The *Supplementary Excel Table* presents the data collected from existing literature sources as well as the reasons why specific measurements were excluded. Further, the calculation of the means is shown in an extra sheet.

References

Azevedo, F.A.C., Carvalho, L.R.B., Grinberg, L.T., Farfel, J., Ferretti, R.E.L., Leite, R.E.P., Filho, W.J., Lent, R., Herculano-Houzel, S., 2009. Equal numbers of neuronal and nonneuronal cells make the human brain an isometrically scaled-up primate brain. J. Comp. Neurol. 513, 532–541. doi:10.1002/cne.21974.

Balasubramanian, V., Kimber, D., Berry, M.J., 2001. Metabolically efficient information processing. Neural Comput. 13, 799–815.

Boddy, A.M., McGowen, M.R., Sherwood, C.C., Grossman, L.I., Goodman, M., Wildman, D.E., 2012. Comparative analysis of encephalization in mammals reveals relaxed constraints on anthropoid primate and cetacean brain scaling. J. Evol. Biol. 25, 981–994. doi:10.1111/j.1420-9101.2012.02491.x.

Bok, S.T., 1929. Der Einfluß der in den Furchen und Windungen auftretenden Krümmungen der Großhirnrinde auf die Rindenarchitektur. Zeitschr. gesamte Neur. Psych. 121, 682–750.

Braitenberg, V., 2001. Brain size and number of neurons: An exercise in synthetic neuroanatomy. J. Comput. Neurosci. 10, 71–77.

Brodmann, K., 1913. Neue Forschungsergebnisse der Großhirnrindenanatomie. Verhandlungen der Gesellschaft Deutscher Naturforscher und Ärzte 85, 200–240.

Carlo, C.N., Stevens, C.F., 2013. Structural uniformity of neocortex, revisited. Proc. Natl. Acad. Sci. USA 110, 1488–1493. doi:10.1073/pnas.1221398110.

Changizi, M.A., 2001. Principles underlying mammalian neocortical scaling. Biol. Cybern. 84, 207–215.

da Costa Campos, L., Hornung, R., Gompper, G., Elgeti, J., Caspers, S., 2020. The role of thickness inhomogeneities in hierarchical cortical folding. bioRxiv 04, 020172. doi:10.1101/2020.04.01.020172.

Cuntz, H., Mathy, A., Häusser, M., 2012. A scaling law derived from optimal dendritic wiring. Proc. Natl. Acad. Sci. USA 109, 11014–11018. doi:10.1073/pnas.1200430109.

Elias, H., Schwartz, D., 1971. Cerebrocortical surface areas, volumes, lengths of gyri and their interdependence in mammals, including man. Z. Säugetierk. 36, 147–163.

Frangou, S., Modabbernia, A., Doucet, G.E., Papachristou, E., Williams, S.C., Agartz, I., Aghajani, M., Akudjedu, T.N., Albajes-Eizagirre, A., Alnæs, D., Alpert, K.I., Andersson, M., Andreasen, N., Andreassen, O.A., Asherson, P., Banaschewski, T., Bargallo, N., Baumeister, S., Baur-Streubel, R., Bertolino, A., Bonvino, A., Boomsma, D.I., Borgwardt, S., Bourque, J., Brandeis, D., Breier, A., Brodaty, H., Brouwer, R.M., Buitelaar, J.K., Busatto, G.F., Buckner, R.L., Calhoun, V., Canales-Rodríguez, E.J., Cannon, D.M., Caseras, X., Castellanos, F.X., Cervenka, S., Chaim-Avancini, T.M., Ching, C.R., Clark, V.P., Conrod, P., Conzelmann, A., Crespo-Facorro, B., Crivello, F., Crone, E.A., Dale, A.M., Davey, C., de Geus, E.J., de Haan, L., de Zubicaray, G.I., den Braber, A., Dickie, E.W., Di Giorgio, A., Doan, N.T., Dørum, E.S., Ehrlich, S., Erk, S., Espeseth, T., Fatouros-Bergman, H., Fisher, S.E., Fouche, J.P., Franke, B., Frodl, T., Fuentes-Claramonte, P., Glahn, D.C., Gotlib, I.H., Grabe, H.J., Grimm, O., Groenewold, N.A., Grotegerd, D., Gruber, O., Gruner, P., Gur, R.E., Gur, R.C., Harrison, B.J., Hartman, C.A., Hatton, S.N., Heinz, A., Heslenfeld, D.J., Hibar, D.P., Hickie, I.B., Ho, B.C., Hoekstra, P.J., Hohmann, S., Holmes, A.J., Hoogman, M., Hosten, N., Howells, F.M., Hulshoff Pol, H.E., Huyser, C., Jahanshad, N., James, A., Jiang, J., Jönsson, E.J., Joska, J.A., Kahn, R., Kalnin, A., Kanai, R., Kang, S., Klein, M., Klushnik, T.P., Koenders, L., Koops, S., Krämer, B., Kuntsi, J., Lagopoulos, J., Lázaro, L., Lebedeva, I., Lee, W.H., Lesch, K.P., Lochner, C., Machielsen, M.W., Maingault, S., Martin, N.G., Martínez-Zalacaín, I., Mataix-Cols, D., Mazoyer, B., McDonald, C., McDonald, B.C., McIntosh, A.M., McMahon, K.L., McPhilemy, G., Menchón, J.M., Medland, S.E., Meyer-Lindenberg, A., Naaijen, J., Najt, P., Nakao, T., Nordvik, J.E., Nyberg, L., Oosterlaan, J., Ortiz-García de la Foz, V., Paloyelis, Y., Pauli, P., Pergola, G., Pomarol-Clotet, E., Portella, M.J., Potkin, S.G., Radua, J., Reif, A., Roffman, J.L., Rosa, P.G., Sacchet, M.D., Sachdev, P.S., Salvador, R., Sànchez-Juan, P., Sarró, S., Satterthwaite, T.D., Saykin, A.J., Serpa, M.H., Schmaal, L., Schnell, K., Schumann, G., Smoller, J.W., Sommer, I., Soriano-Mas, C., Stein, D.J., Strike, L.T., Swagerman, S.C., Tamnes, C.K., Temmingh, H.S., Thomopoulos, S.I., Tomyshev, A.S., Tordesillas-Gutiérrez, D., Trollor, J.N., Turner, J.A., Uhlmann, A., van den Heuvel, O.A., van den Meer, D., van der Wee, N.J., van Haren, N.E., van 't Ent, D., van Erp, T.G., Veer, I.M., Veltman, D.J., Völzke, H., Walter, H., Walton, E., Wang, L., Wang, Y., Wassink, T.H., Weber, B., Wen, W., West, J.D., Westlye, L.T., Whalley, H., Wierenga, L.M., Wittfeld, K., Wolf, D.H., Wright, M.J., Yang, K., Yoncheva, Y., Zanetti, M.V., Ziegler, G.C., Thompson, P.M., Dima, D., 2020. Cortical thickness trajectories across the lifespan: Data from 17,075 healthy individuals aged 3-90 years. bioRxiv doi:10.1101/2020.05.05.077834.

Garcia, K.E., Robinson, E.C., Alexopoulos, D., Dierker, D.L., Glasser, M.F., Coalson, T.S., Ortinau, C.M., Rueckert, D., Taber, L.A., Van Essen, D.C., Rogers, C.E., Smyser, C.D., Bayly, P.V., 2018. Dynamic patterns of cortical expansion during folding of the preterm human brain. Proc. Natl. Acad. Sci. USA 115, 3156–3161. doi:10.1073/pnas.1715451115.

Haug, H., 1970. Der makroskopische Aufbau des Großhirns: Qualitative und quantitative Untersuchungen an den Gehirnen des Menschen, der Delphinoideae und des Elefanten. Springer, Berlin.

Henneberg-Neubabelsberg, R., 1910. Messungen der Oberfläche der Großhirnrinde. J. f. Psychol. u. Neurol. 17, 144–158.

Herculano-Houzel, S., 2012. The remarkable, yet not extraordinary, human brain as a scaled-up primate brain and its associated cost. Proc. Natl. Acad. Sci. USA 109, 10661–10668. doi:10.1073/pnas.1201895109.

Hofman, M.A., 1985. Size and shape of the cerebral cortex in mammals. I. The cortical surface. Brain Behav. Evol. 27, 28–40.

Hofman, M.A., 1989. On the evolution and geometry of the brain in mammals. Prog. Neurobiol. 32, 137–158. doi:10.1016/0301-0082(89)90013-0.

Hofman, M.A., 1991. The fractal geometry of convoluted brains. J. Hirnforsch. 32, 103–111.

Jerison, H.J., 1979. The evolution of diversity of brain size, in: M. E. Hahn, C.J., Dudek, B.C. (Eds.), Development and Evolution of Brain Size: Behavioral Implications, Academic Press, New York. pp. 30–60.

Kaas, J.H., 2011. Reconstructing the areal organization of the neocortex of the first mammals. Brain Behav. Evol. 78, 7–21. doi:10.1159/000327316.

Kapellou, O., Counsell, S.J., Kennea, N., Dyet, L., Saeed, N., Stark, J., Maalouf, E., Duggan, P., Ajayi-Obe, M., Hajnal, J., Allsop, J.M., Boardman, J., Rutherford, M.A., Cowan, F., Edwards, A.D., 2006. Abnormal cortical development after premature birth shown by altered allometric scaling of brain growth. PLOS Medicine 3, 1–9. doi:10.1371/journal.pmed.0030265.

Karbowski, J., 2003. How does connectivity between cortical areas depend on brain size? implications for efficient computation. J. Comput. Neurosci. 15, 347–356. doi:10.1023/A:1027467911225.

Koch, K., McLean, J., Segev, R., Freed, M.A., Berry II, M.J., Balasubramanian, V., Sterling, P., 2006. How much the eye tells the brain. Curr. Biol. 16, 1428–1434. doi:10.1016/j.cub.2006.05.056.

Le Gros Clark, W., 1945. Deformation patterns on the cerebral cortex, in: Essays on growth and form, Oxford University Press, Oxford. pp. 1–22.

de Lussanet, M.H.E., 2015. How the flow and processing of information shapes the cerebrum. PeerJ PrePrints 3, e1518. doi:10.7287/peerj.preprints.239v2.

de Lussanet, M.H.E., 2016. Comment on "Cortical fold-

ing scales universally with surface area and thickness, not number of neurons". Science 351, 825. doi:10.1126/science.aad0127.

Manger, P.R., 2006. An examination of cetacean brain structure with a novel hypothesis correlating thermogenesis to the evolution of a big brain. Biol. Rev. 81, 293–338. doi:10.1017/S1464793106007019.

Manger, P.R., 2013. Questioning the interpretations of behavioral observations of cetaceans: Is there really support for a special intellectual status for this mammalian order? Neuroscience 250, 664–696. doi:10.1016/j.neuroscience.2013.07.041.

Manger, P.R., Prowse, M., Haagensen, M., Hemingway, J., 2012. Quantitative analysis of neocortical gyrencephaly in african elephants (loxodonta africana) and six species of cetaceans: comparison with other mammals. J. Comp. Neurol. 520, 2430–2439. doi:10.1002/cne.23046.

Manyuhina, O.V., Mayett, D., Schwarz, J.M., 2014. Elastic instabilities in a layered cerebral cortex: A revised axonal tension model for cortex folding. New Journal of Physics 16, 123058. doi:10.1088/1367-2630/16/12/123058.

Marino, L., Connor, R.C., Fordyce, R.E., Herman, L.M., Hof, P.R., Lefebvre, L., Lusseau, D., McCowan, B., Nimchinsky, E.A., Pack, A.A., Rendell, L., Reidenberg, J.S., Reiss, D., Uhen, M.D., Van der Gucht, E., Whitehead, H., 2007. Cetaceans have complex brains for complex cognition. PLoS Biol. 5, 966–972.

Mayhew, T.M., Mwamengele, G.L., Dantzer, V., 1996. Stereological and allometric studies on mammalian cerebral cortex with implications for medical brain imaging. J. Anat. 189, 177–184.

Mota, B., Herculano-Houzel, S., 2012. How the cortex gets its folds: An inside-out, connectivity-driven model for the scaling of Mammalian cortical folding. Front. Neuroanat. 6, 3. doi:10.3389/fnana.2012.00003.

Mota, B., Herculano-Houzel, S., 2015. Cortical folding scales universally with surface area and thickness, not number of neurons. Science 349, 74–77. doi:10.1126/science.aaa9101.

Patzke, N., Spocter, M.A., Karlsson, K.Æ., Bertelsen, M.F., Haagensen, M., Chawana, R., Streicher, S., Kaswera, C., Gilissen, E., Alagaili, A.N., Mohammed, O.B., Reep, R.L., Bennett, N.C., Siegel, J.M., Ihunwo, A.O., Manger, P.R., 2015. In contrast to many other mammals, cetaceans have relatively small hippocampi that appear to lack adult neurogenesis. Brain Struct. Funct. 220, 361–383. doi:10.1007/s00429-013-0660-1.

Perge, J.A., Koch, K., Miller, R., Sterling, P., Balasubramanian, V., 2009. How the optic nerve allocates space, energy capacity, and information. J. Neurosci. 29, 7917–7928.

Perge, J.A., Niven, J.E., Mugnaini, E., Balasubramanian, V., Sterling, P., 2012. Why do axons differ in caliber? J. Neurosci. 32, 626–638. doi:10.1523/jneurosci.4254-11.2012.

Pilleri, G., Gihr, M., 1970. The central nervous system of the Mysticete and Odontocete whales. Investigations on Cetacea 2, 89–135.

Prothero, J.W., Sundsten, J.W., 1984. Folding of the cerebral cortex in mammals: a scaling model. Brain Behav. Evol. 24, 152–167.

Rakic, P., 1995. A small step for the cell, a giant leap for mankind: a hypothesis of neocortical expansion during evolution. Trends Neurosci. 18, 383–388. doi:10.1016/0166-2236(95)93934-P.

Rakic, P., 2009. Evolution of the neocortex: a perspective from developmental biology. Nature Reviews Neuroscience 10, 724–735. doi:10.1038/nrn2719.

Rockel, A.J., Hiorns, R.W., Powell, T.P.S., 1980. The basic uniformity in structure of the neocortex. Brain 103, 221–244. doi:10.1093/brain/103.2.221.

Roth, G., 2015. Convergent evolution of complex brains and high intelligence. Philosophical Transactions of the Royal Society of London B: Biological Sciences 370, 49. doi:10.1098/rstb.2015.0049.

Schlenska, G., 1969. Messungen der Oberfläche und der Volumenanteile des Gehirnes menschlicher Erwachsener mit neuen Methoden. Z. Anat. Entwickl. Gesch. 128, 47–59.

Schlenska, G., 1974. Volumen- und Oberflächenmessungen an Gehirnen verschiedener Säugetiere im Vergleich zu einem errechneten Modell. J. Hirnforsch. 15, 401–408.

Stoop, R.L., Saase, V., Wagner, C., Stoop, B., Stoop, R., 2013. Beyond scale-free small-world networks: Cortical columns for quick brains. Phys. Rev. Lett. 110, 108105. doi:10.1103/PhysRevLett.110.108105.

Striedter, G.F., Srinivasan, S., Monuki, E.S., 2015. Cortical folding: When, where, how, and why? Ann. Rev. Neurosci. 38, 291–307. doi:10.1146/annurev-neuro-071714-034128.

Todd, P.H., 1982. A geometric model for the cortical folding pattern of simple folded brains. Journal of Theoretical Biology 97, 529 – 538. URL: http://www.sciencedirect.com/science/article/pii/0022519382903800, doi:https://doi.org/10.1016/0022-5193(82)90380-0.

Toro, R., Perron, M., Pike, B., Richer, L., Veillette, S., Pausova, Z., Paus, T., 2008. Brain size and folding of the human cerebral cortex. Cereb. Cortex 18, 2352–2357. doi:10.1093/cercor/bhm261.

Van Essen, D.C., 1997. A tension-based theory of morphogenesis and compact wiring in the central nervous system. Nature 385, 313–318. doi:10.1038/385313a0.

Van Essen, D.C., Donahue, C.J., Coalson, T.S., Kennedy, H., Hayashi, T., Glasser, M.F., 2019. Cerebral cortical folding, parcellation, and connectivity in humans, nonhuman primates, and mice. Proc. Natl. Acad. Sci. USA 116, 26173–26180. doi:10.1073/pnas.1902299116.

Wang, X., Studholme, C., Grigsby, P.L., Frias, A.E., Cuzon Carlson, V.C., Kroenke, C.D., 2017. Folding, but not surface area expansion, is associated with cellular morphological maturation in the fetal cerebral cortex. J. Neurosci. 37, 1971–1983. URL: https://www.jneurosci.org/content/37/8/1971, doi:10.1523/jneurosci.3157-16.2017.

Xu, G., Knutsen, A.K., Dikranian, K., Kroenke, C.D., Bayly, P.V., Taber, L.A., 2010. Axons pull on the brain, but tension does not drive cortical folding. J. Biomech. Eng. 132, 071013. doi:10.1115/1.4001683.

Zhang, K., Sejnowski, T.J., 2000. A universal scaling law between gray matter and white matter of cerebral cortex. Proc. Natl. Acad. Sci. USA 97, 5621–5626. doi:10.1073/pnas.090504197.

Supplementary material

Methods

Dataset

The supplementary excel table presents the data collected from existing literature sources as well as the reasons why specific measurements were excluded. Further, the calculation of the means is shown in an extra sheet.

First order model: Fractal-like growth rule for gyrification

The first order model neglects the white matter contribution to the cerebral volume. It is based on the central hypothesis of a homogeneous composition of the cortex (ETH). Accordingly, the thickness of the cortex is limited, so once the critical thickness is reached, growth is only possible if the cortex invaginates, to form a sulcus (Fig. S3A). If the cerebrum exceeds a critical size (inner section "1" in Fig. S3A), a sulcus is initiated, but as long as it is smaller than the critical size, its surface is smooth (lissencephalic).

According to the first model, growth only occurs on the apex of each gyrus, and so the valley of a sulcus, once formed, will not move away from the center. Thus, the number of sulci decreases linearly when moving from the surface to the center of the cerebrum.

Note, that for very small cerebrums, the surface is entirely on the outside, so the cortical surface A scales to the cerebral volume V according to an isometric scaling law: $A = cV$ (with c being a constant). On the other hand, for very large cerebrums, most of the cortical surface lies within the sulci, and since the thickness of the gyri remains constant, the surface will scale to the volume in a linear manner. Thus, the model will interpolate between the two scaling laws: a 2/3 power law for very small cerebrums and a linear scaling for very large ones (cf. Fig. S3B).

Note that this simple, first order model is just two-dimensional (2D), which is sufficiently realistic, though, because primary fields are elongated, so that gyri and sulci are elongated as well.

Analytically, the total circumference C of the 2D model is the sum of the exposed and non-exposed (inward) circumferences, which can be calculated as: $C = (2\pi R) + (\frac{2\pi}{d_{\text{crit}}} R^2 - R)$ for a circle with radius R and straight sulci. Additionally, a shape constant can be introduced to account for the deviation of an exact circular shape of the model, the 3D version of the model will thus be of the general form: $C = R^2/d + sR$, where d has the dimension of length and is related to the critical distance d_{crit}, and where s is a dimensionless shape parameter.

When adding the third dimension, the total circumference becomes the total cortical surface A. The exposed surface will scale with the volume V to the 2/3 power in analogy to the surface of a sphere, so $V \sim R^3$, whereas the non-exposed, inward folded surface scales again linearly with the volume (as a result of the invariant gyral thickness), so $V \sim A^{3/2}$. In summary, the 3D version of the model is of the general form $V = A^{3/2}/d + sA$, where d is, again, a thickness parameter with the dimension of length, and where s is a dimensionless shape parameter. Note that d and s in the 2D and 3D models are different but analogous parameters.

Supplementary Results

Figures S1-S3 present supplementary results.

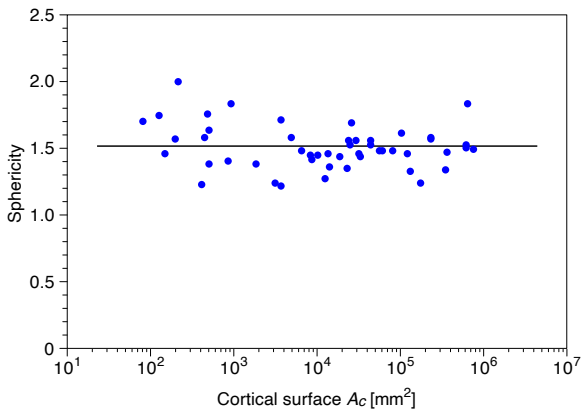

Figure S1: Sphericity of a 3D shape is defined as the ratio of the exposed surface (A_{exp}) to the surface area of a sphere expressed in terms of its volume: $s = A_{exp}/\sqrt[3]{36\pi V^2}$)). The equation for the surface area of a sphere of volume V can be calculated by solving the standard equations for it surface area ($A_{\text{sphere}} = 4\pi R^2$) and volume ($V_{\text{sphere}} = 4/3\pi R^3$). According to the database, the mean $s = 1.57 \pm 0.16$ (st.dev.) for the mammalian cerebrum (N=43 species, 66 specimen; see supplementary Excel Table).

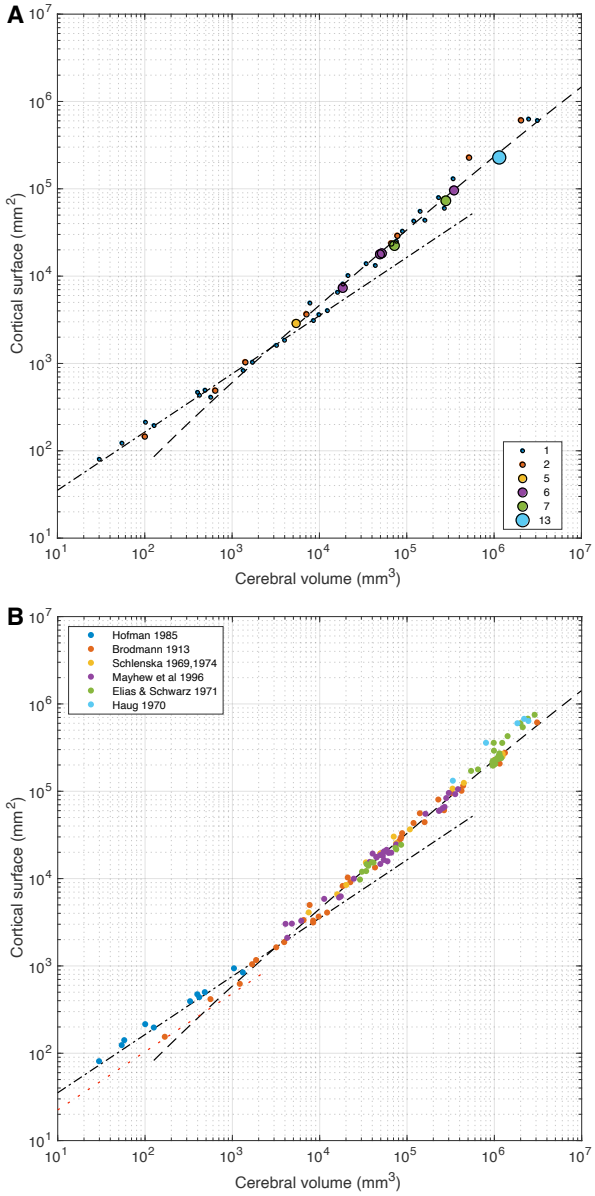

Figure S2: Supplemental Figure: Model for the cortical surface in relation to the cerebral volume (cf. Fig. 2). A. By no of specimen per species: the size of each icon represents the number of specimen included for each species. Humans are represented by the largest number, but note, that the MRI data of Toro et al. (2008) was not included in the statistics. B. By reference. The individual specimen are each shown as a single dot. Note, that the surface area cannot be smaller than the surface area of a sphere of the same volume (i.e., the sphericity $s > 1$, see Fig. S1). This limit is shown by the red dotted line.

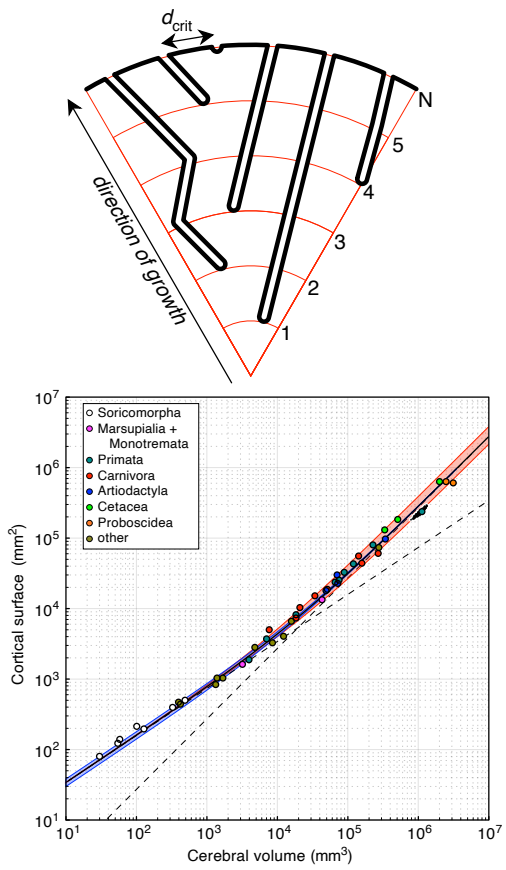

Figure S3: A. Schema of fractal-like growth rule approximation: The cortical surface (thick black curve) is on the exposed outside as well as in the sulci. Each time the gyral width exceeds the critical width (d_{crit}), a new sulcus is formed. By this rule, the number of sulci, N, increases with the radius of the cerebrum. Note, that a small cerebrum with not have any sulci and will thus be lissencephalic (smooth). B. Behavior of this first order approximation on a logarithmic scale. Each dot represents the mean of one species (human data are in addition shown as a cloud). On a logarithmic scale, the model approaches two asymptotes: $A = 7.1V^{2/3}$ (isometric scaling relation), $A = 0.22V$ (linear relation). Blue and red shades: influence of 1 standard deviation for each of the two fitting parameters.